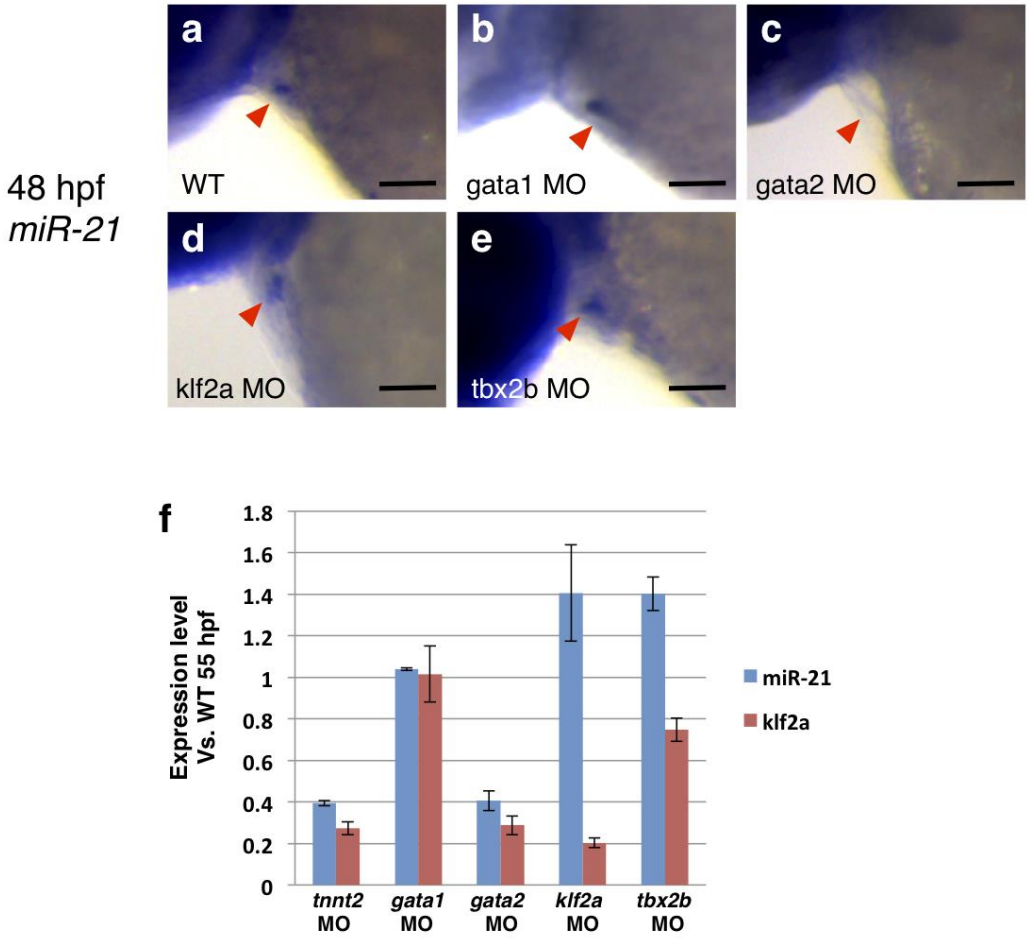

Supplementary Figure S1. Effects of knocking-down of *gata1*, *gata2*, *klf2a* and *tbx2b* on the expression of *miR-21*.

(**a**) The normal expression of *miR-21* in the valve-forming endocardial cells in the WT at 48 hpf. (**b**) Injection of the *gata1* MO did not affect the expression of *miR-21*. (**c**) The *miR-21* expression disappeared after injection of the *gata2* MO. (**d** and **e**) Injection of neither the *klf2a* (**d**) or *tbx2b* MO (**e**) affected the *miR-21* expression. (**f**) Effects of injection of several MOs on the expression of *miR-21* and *klf2a*, both of which are expressed in the valve-forming endocardial cells in a flow-dependent manner. Expression levels were measured by qRT-PCR using RNA isolated from the hearts. In both the *tnnt2* and *gata2* morphants, *miR-21* and *klf2a* were suppressed to 20 to 40%, whereas the *gata1* MO failed to repress them. Error bars represent mean±SEM. Scale bars, 50μm.

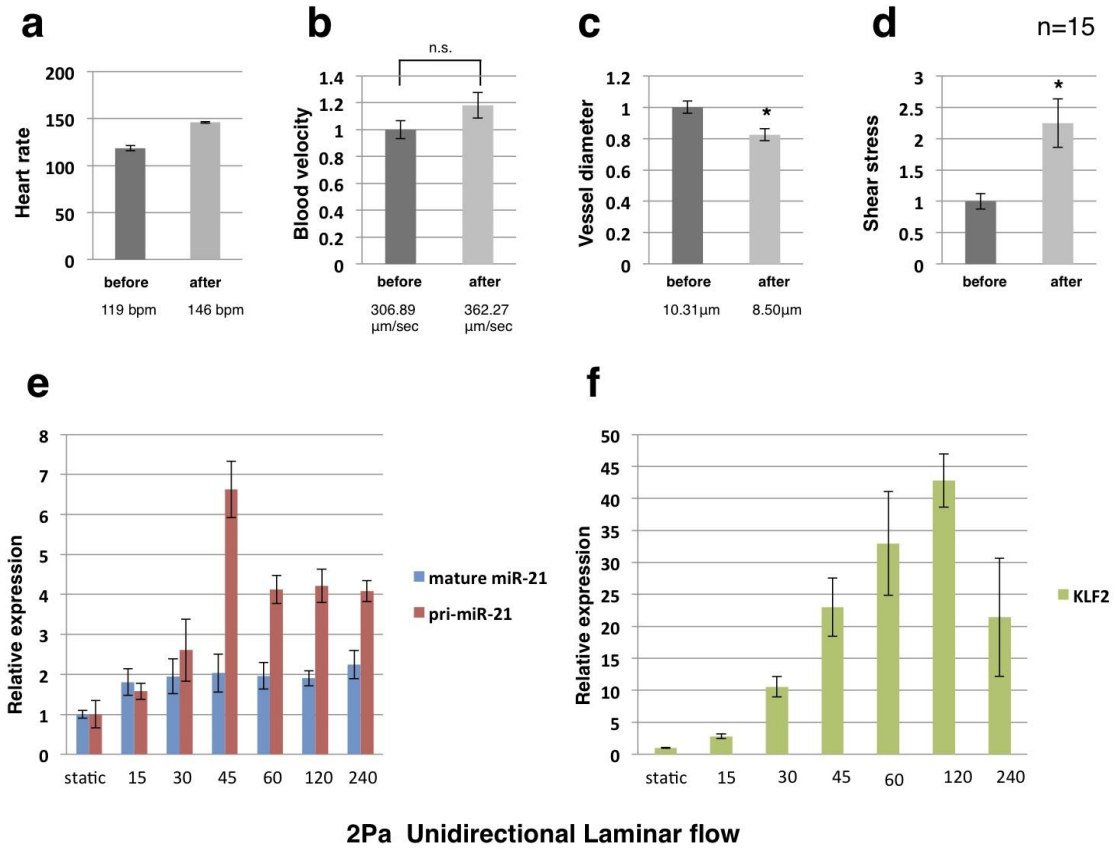

Supplementary Figure S2a - f. Changes in hemodynamics parameters and effects of unidirectional laminar flow before and after the epinephrine treatment.

(**a**) Heart rate was increased from 119 to 146 beats per minute (bpm) by the epinephrine stimulation. (**b**) Blood velocity was measured at the head vasculature (middle cerebral vein). The circulation velocity became slightly faster after the stimulation (from 306.89 to 362.27 µm/sec), but this change was not significant. (**c**) Blood vessel became narrower after the treatment from 10.31 to 8.50µm. (**d**) The shear stress calculated from these data (the shear stress $\tau = 4\mu Q / \pi a^3$, see Materials) increased approximately 2 fold. (**e**) Induction profiles of the *pri-miR-21* and mature *miR-21* in HUVECs by 2.0 Pa of unidirectional laminar flow. Induction of the *pri-miR-21* was robust and hit the peak 45 min after application of the flow. The mature *miR-21* was also induced rapidly, but kept low. (**f**) Induction of *KLF2* was also rapid and robust, but showed a gradual increase with the highest peak after 120 min. Error bars represent mean±SEM.

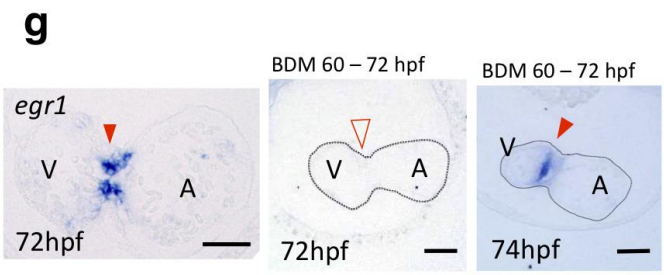

h

	expression in zebrafish heart
miR-21	Valves
klf2a	
egr1	
bmp4	
notch1b	
has2	
miR-23	
miR-24	
miR-150	
miR-126	Whole heart
miR-138	Ventricular myocardium
miR-143	Ventricle and outflow tract
miR-145	Outflow tract

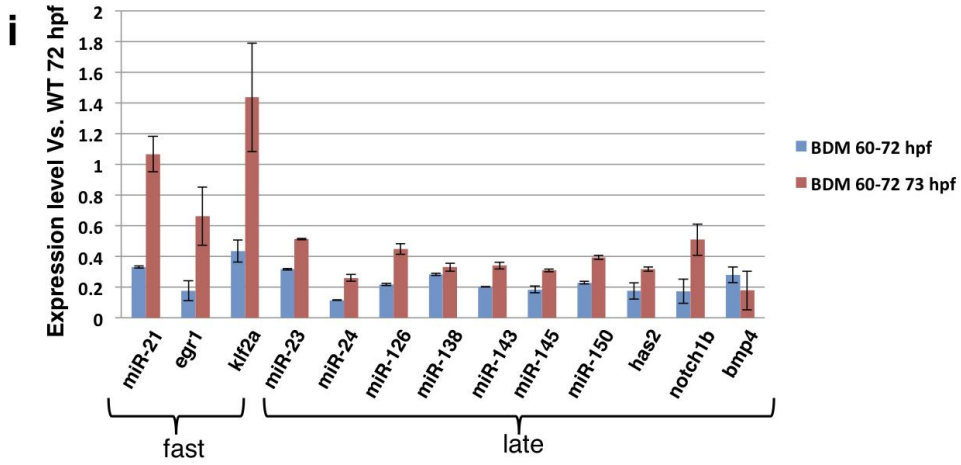

Supplementary Figure S2g - i. Effects of BDM treatment.

(**g**) *egr1* (*early growth response 1*) is expressed in the valve-forming endocardium at the AV canal (left panel). 12 hr arrest of the heartbeat erased this expression (middle panel), but a short period of the heartbeat restored it (right panel). Scale bars, 50μm. (**h**) A list of cardiac genes checked for the heartbeat-dependency. (**i**) Zebrafishs were treated with BDM from 60 to 72 hps to stop the heartbeat. For a half of fishes, BDM was washed away to restart the heartbeat for 1 hr. RNA samples were isolated from the hearts, then subjected to the qRT-PCR assay. *miR-21*, *egr1* and *klf2a* respond to the re-initiated heartbeat rapidly, but expression of other genes was not restored by a short period of the heartbeat. Error bars represent mean±SEM.

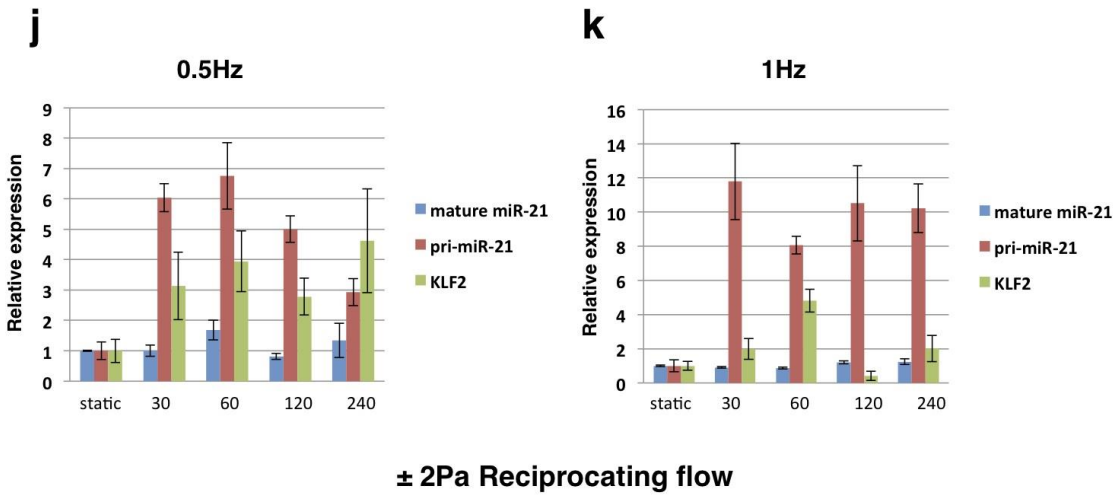

Supplementary Figure S2j and k. Effects of reciprocating flow. (**j** and **k**) Induction of the *pri-miR-21*, mature *miR-21* and *KLF2* in HUVECs by 2.0 Pa of the reciprocating flow. Induction of the *pri-miR-21* was fast and robust, and hit the maximal level within 30 min, whereas that of the mature *miR-21* was kept low. Induction of *KLF2* was different when reciprocating flow was applied. The *pri-miR-21* responded similarly to both 0.5 and 1.0 Hz of reciprocating flow, yet the *KLF2* induction by 1.0 Hz flow was weaker. Error bars represent mean±SEM.

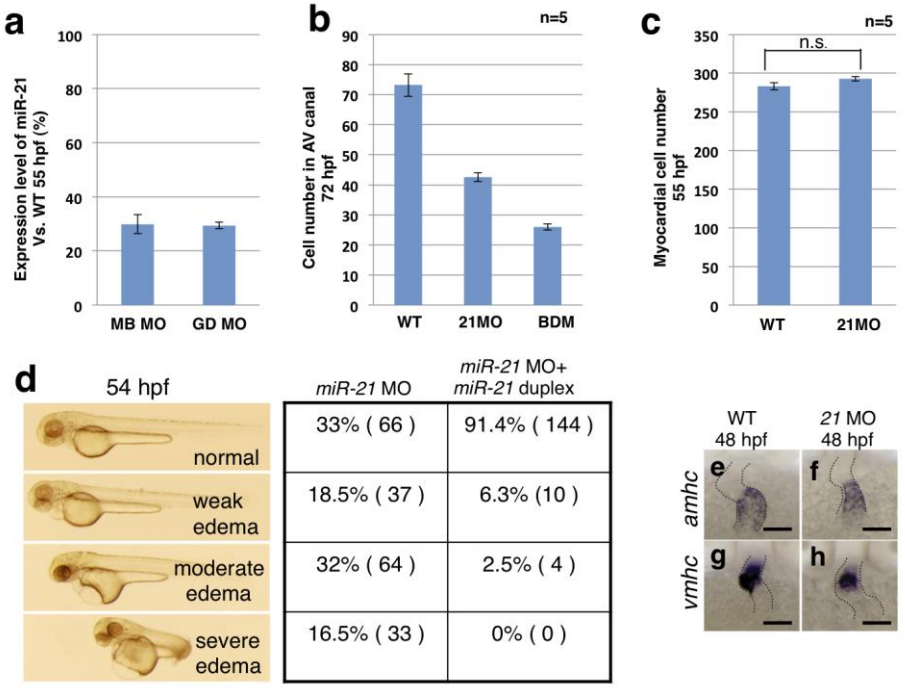

Supplementary Figure S3. Cell numbers, rescue experiments and AV markers in the morphants.

(**a**) Confirmation of the effectiveness of two *miR-21* MOs by qRT-PCR on cDNA templates prepared from the whole bodies; the multi-blocking and Guide Dicer MOs (MB MO and GD MO, respectively). Both MOs repressed the expression of *miR-21* by approximately 70%. Error bars represent mean±SEM. (**b**) Cell numbers of the endocardial cells at the AV canal were counted at 72 hpf. The WT hearts have approximately 70 endocardial cells at the AV canal, while the *miR-21* morphants and BDM-treated hearts possess only 43 and 26 cells, respectively. (**c**) In contrast to the endocardial cell loss, myocardical cells were not affected. (**d**) Rescue experiments using a *miR-21* duplex. Phenotypes induced by injection of the *miR-21* MO were classified into four categories from normal morphology to severe edema. Injection of the *miR-21* MO resulted in an edematous appearance in 67% of the injected embryos (18.5% weak, 32% moderate and 16.5% severe). When the *miR-21* duplex was co-injected, the edematous phenotypes were induced in 8.8% of embryos (6.3% weak, 2.5% moderate and 0% severe) with 91.4% of embryos showing normal blood circulation. (**e** to **h**) The atrial markers (*amhc*; *atrial myosin heavy chain* in **e** and **f**) and the ventricular markers (*vmhc*; *ventricular myosin heavy chain* in **g** and **h**) were expressed in the same patterns in the *miR-21* morphants (**f** and **h**) and the WT (**e** and **g**). Scale bars, 50μm.

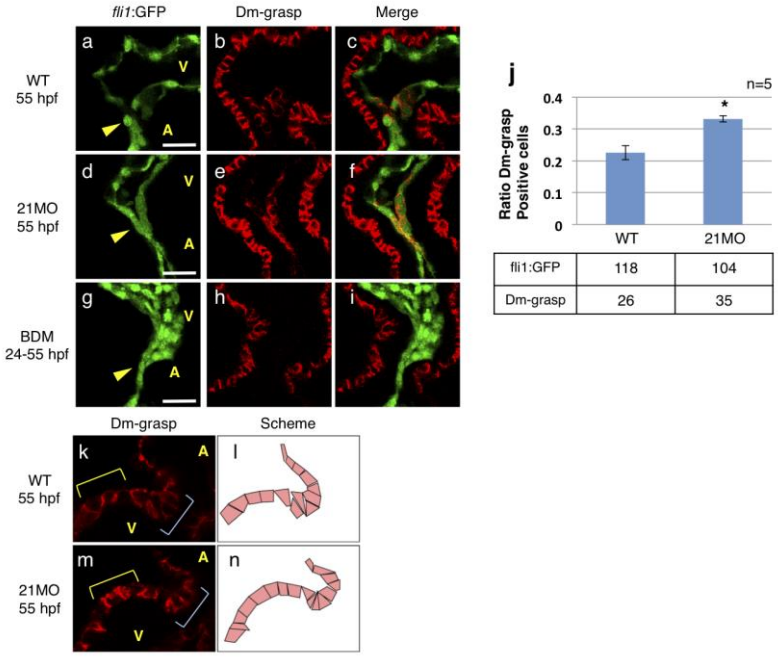

Supplementary Figure S4. Visualization of cells.

(**a** to **c**) Cells were visualized by GFP driven by the *fli1* promoter and Dm-grasp staining at 55 hpf. At the AV junction (yellow arrowhead), the valve-forming endocardial cells (GFP- and Dm-grasp-double positive) were round and cuboidal, making a compact aggregation of cells. (**d** to **f**) In the *miR-21* morphants, cells were flattened, and only a stretched layer of cells was formed, rather than a lump of cuboidal cells. (**g** to **i**) The heartbeat arrest by BDM induced a similar phenotype as the *miR-21* morphants, yet the number of Dm-grasp-positive cells was strikingly decreased. Scale bars, 20μm (**a**, **d** and **g**). (**j**) Ratios of the Dm-grasp-positive cells to the GFP-positive ones were estimated. In the WT at 55 hpf, the GFP-positive and Dm-grasp-positive cells were 118 and 26 at the AV junction, respectively. Hence, approximately 20% of cells were Dm-grasp-positive. In the *miR-21* morphants, the number of the GFP-positive cells was slightly decreased (from 118 to 104), whereas the Dm-grasp-positive cells increased (from 26 to 35). Consequently, approximately 30% of cells were Dm-grasp-positive. Error bars represent mean±SEM. (**k** to **n**) Cell shapes of cardiomyocytes are visualized by Dm-grasp staining. In the WT, cardiomyocytes at the AV junction constrict their apical surface and show a trapezoidal or triangular appearance (blue line in **k**), whereas atrial and ventricular cardiomyocytes are squamous and cuboidal (yellow line). This characteristic cell shapes were also observed in the *miR-21* morphants (**m**). A schematic representation is shown in **l** and **n**.

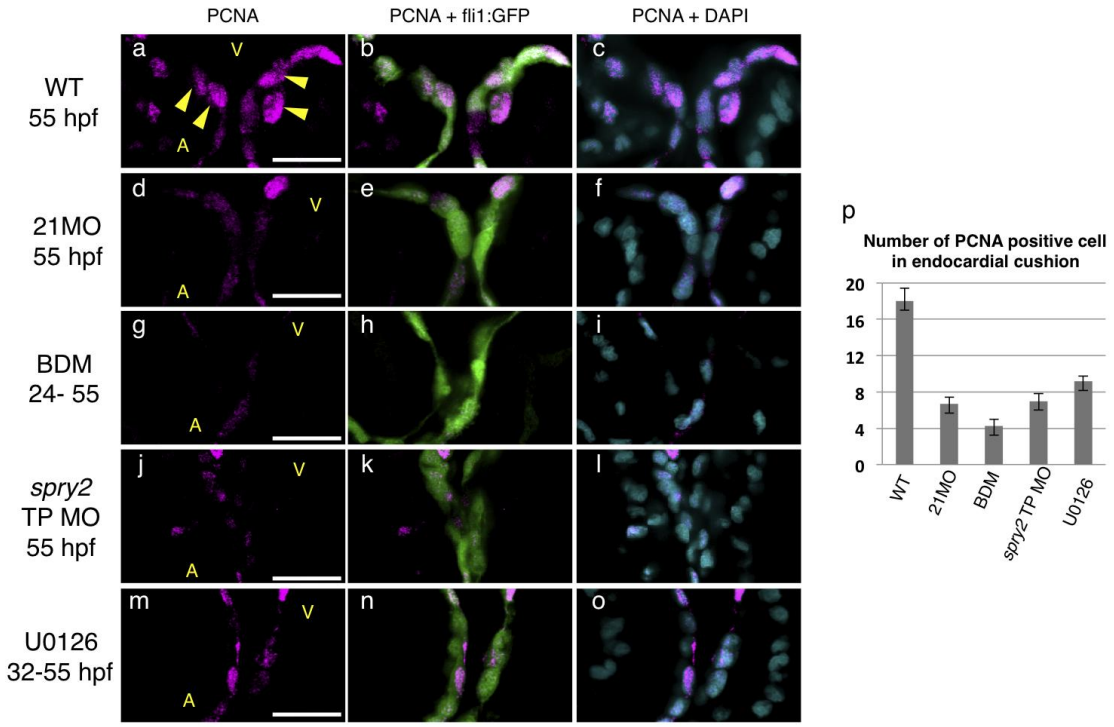

Supplementary Figure S5. Expression of pcna.

Expression of pcna proteins was examined. (**a** to **c**) In the WT, pcna proteins were clearly detected in the valve-forming endocardial cells labeled by GFP driven by the *fli1* promoter (yellow arrowheads in **a**). DAPI staining was also performed to visualize nuclei (**c**). (**d** to **f**) In the *miR-21* morphants, expression of pcna was significantly reduced. A loss of or significant reduction of the pcna expression was also evident in the BDM-treated hearts (**g** to **i**), *spry2* target protector morphants (**j** to **l**) and U0126-treated embryos (**m** to **o**). Scale bars, 20μm. (**p**) Numbers of the pcna-positive endocardial cells at the AV canal were counted. Reduction of more than 50% was observed in these embryos. Approximately 17 pcna-positive cells were counted in the WT, whereas they are less than 8 in the morphants and drug-treated embryos. Error bars represent mean±SEM.

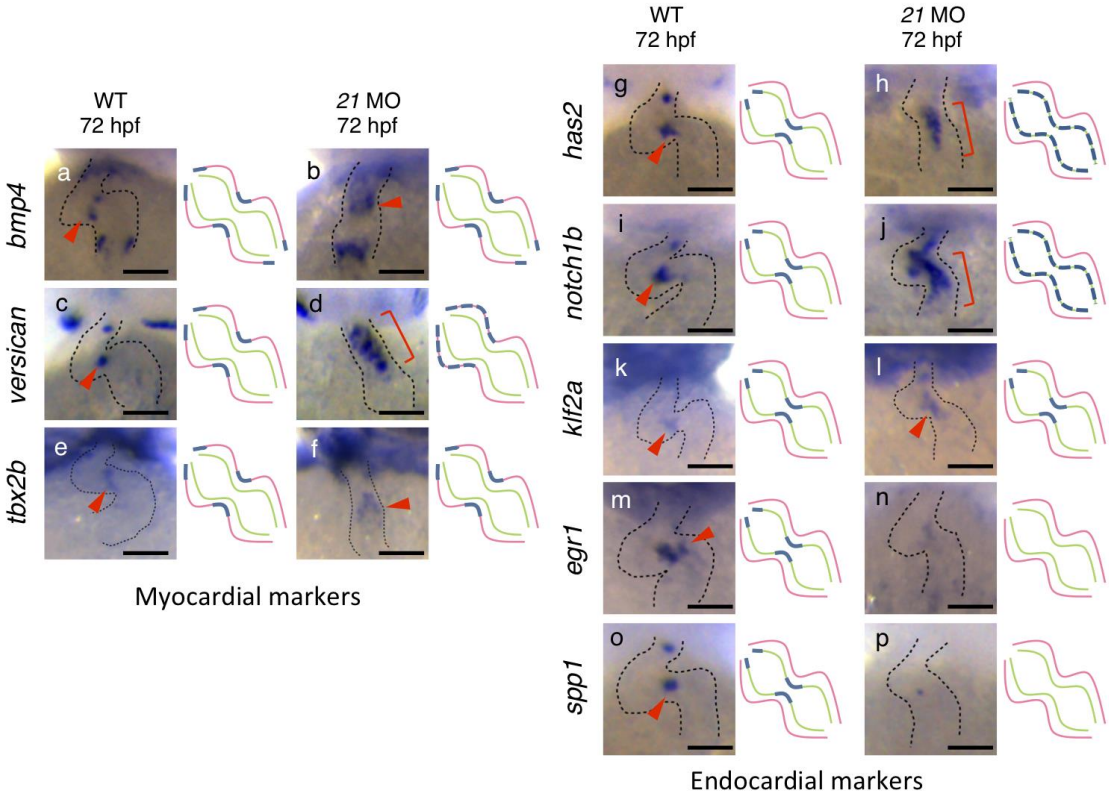

Supplementary Figure S6. Expression patterns of cardiac markers.

(**a** to **f**) Expression patterns of three myocardial markers (*bmp4*, *versican* and *tbx2b*) in the WT (**a**, **c** and **e**) and *miR-21* morphants (**b**, **d** and **f**). Expression of *bmp4* and *tbx2b* was not affected (**a** and **b**, **e** and **f**, respectively). Expression of *versican* was expanded into the ventricle (**c** and **d**). (**g** to **p**) Expression patterns of five endocardial markers (*has2*, *notch1b*, *klf2a*, *egr1* and *spp1*) in the WT and *miR-21* morphants. Expression of *has2* and *notch1b* was expanded into both the atrial and ventricular compartments (**g** and **h**, **i** and **j**, respectively). Expression of *klf2a* was not affected, confined to the two valve-forming points (**k** and **l**). Expression of *egr1* and *spp1* was repressed (**m** and **n**, **o** and **p**, respectively). Scale bars, 50μm.

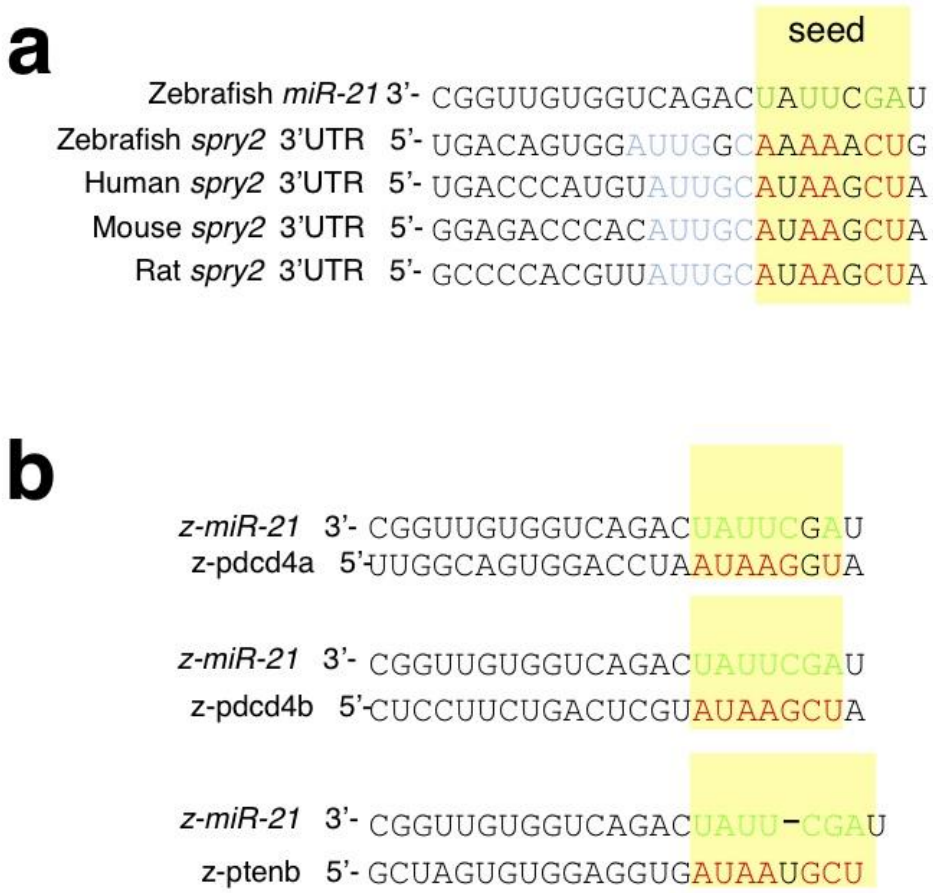

Supplementary Figure S7a and b. Sequence alignments of *miR-21* and its targets. (**a**) Alignments of zebrafish *miR-21* and the 3' un-translated regions (UTRs) of zebrafish, human, mouse and rat *Sprouty 2* (*Spry2*). Seed sequences and nucleotides complementary to *miR-21* are highlighted by colours. (**b**) Alignments of zebrafish *miR-21*, *pdcd4a*, *pdcd4b* and *ptenb*.

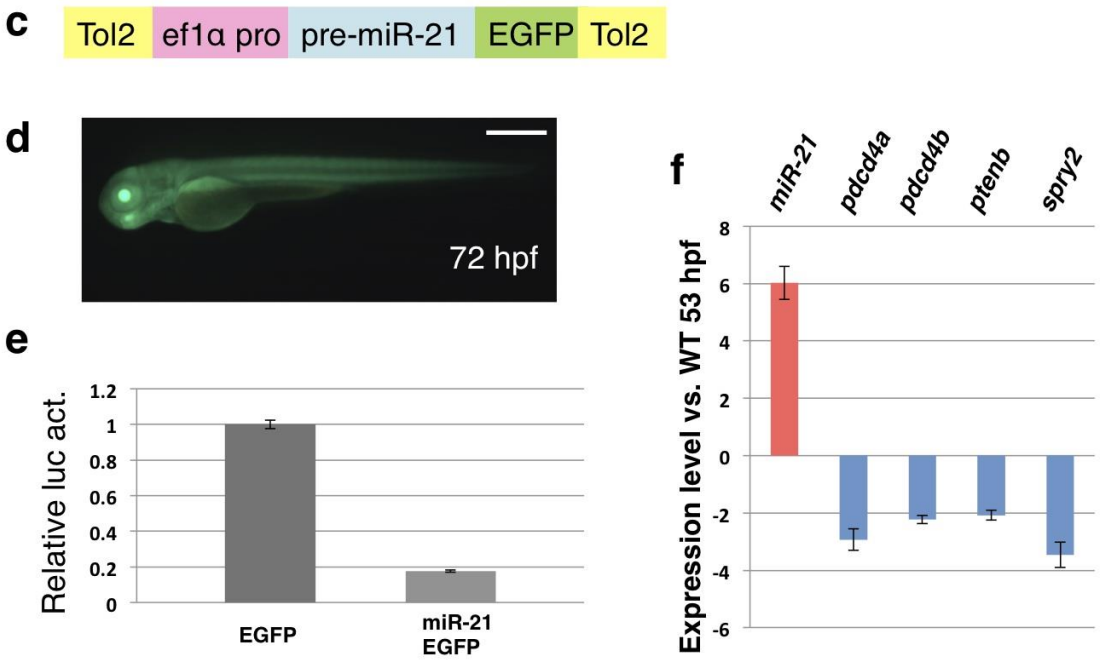

Supplementary Figure S7c - f. Transgenic fish expressing *miR-21*.

(**c**) A schematic representation of a Tol2 transposon vector designed to over-express *pre-miR-21* along with *EGFP* by the *ef1α* (*eukaryotic translation elongation factor 1 alpha*) promoter. (**d**) Expression of *pre-miR-21* was assessed by the fluorescent signals of EGFP. This embryo is F1. Scale bar, 500μm. (**e**) To confirm whether the artificial vector in (**c**) expresses functional *miR-21*, a luciferase assay was performed in HEK293T cells. This vector successfully inhibited more than 80% of the activity of a luciferase reporter that harbours a *z-miR-21* targeting sequence in its 3'UTR. Error bars represent mean±SEM. (**f**) Expression levels of the *miR-21* target genes were measured by qRT-PCR using RNAs isolated from whole bodies of the WT and embryos expressing *pre-miR-21-EGFP*. Expression of the mature *miR-21* was increased approximately 6 fold. Expression of *pdcd4a*, *pdcd4b*, *ptenb* and *spry2* was repressed by approximately 50 to 70%. Error bars represent mean±SEM.

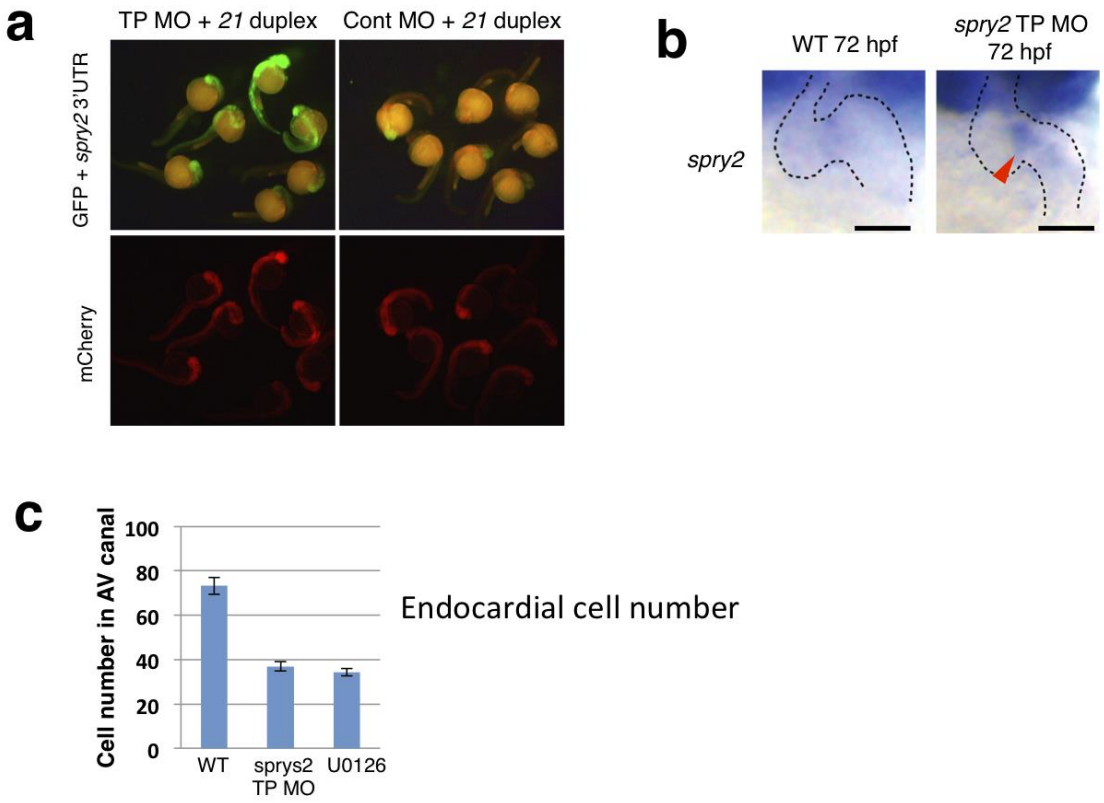

Supplementary Figure S8. *spry2* target protector MO.

(**a**) Efficiency of *spry2* target protector MO (TP-MO) was confirmed. Two mRNAs, one with *GFP* and the *spry2* 3'-UTR as a reporter and another with *mCherry* without the *miR-21* target as an internal control, were used along with the *miR-21* duplex. When a control scrambled MO was co-injected, GFP fluorescent signals were not observed or very week (upper right panel). Co-injection of the *spry2* TP-MO against *miR-21* recovered the expression of GFP (upper left panel). In both cases, mCherry expression was evident equally. (**b**) In the WT hearts, *spry2* was not expressed at 72 hpf. Injection of the *spry2* TP-MO induced expression of *spry2* in the AV canal (red arrowhead). Scale bars, 50μm. (**c**) Injection of the *spry2* TP-MO and U0126 treatment significantly reduced the numbers of the endocardial cells at the AV canal. Error bars represent mean±SEM.

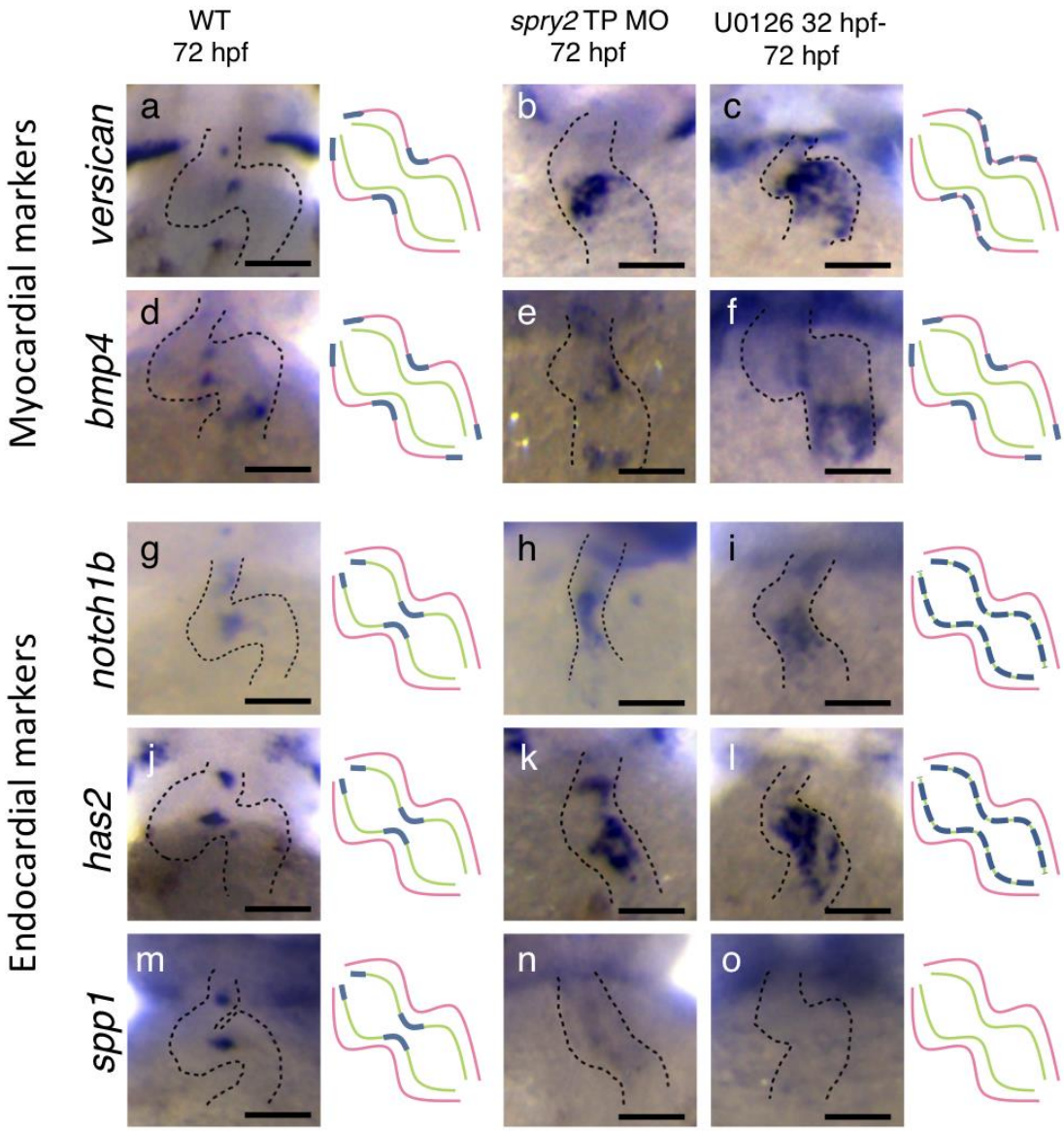

Supplementary Figure S9. Expression patterns of cardiac markers.

Expression of the myocardial (*versican* and *bmp4*) and endocardial marker genes (*notch1b*, *has2* and s*pp1*) in the *spry2* target protector morphants (*spry2* TP MO) and embryos treated by U0126 from 32 to 72 hpf. Normal expression patterns are show in the left (**a**, **d**, **g**, **j** and **m**). Expression of *versican* was expanded both in the *spry2* TP MO and U0126 treatment (**b** and **c**, respectively). Expression of *bmp4* was not affected (**e** and **f**). Expression of *notch1b* (**h** and **i**) and *has2* (**k** and **l**) was expanded. Expression of *spp1* was suppressed (**n** and **o**). These changes of expression are basically similar to the *miR-21* morphants (see Supplementary Figure S6). Scale bars, 50μm.

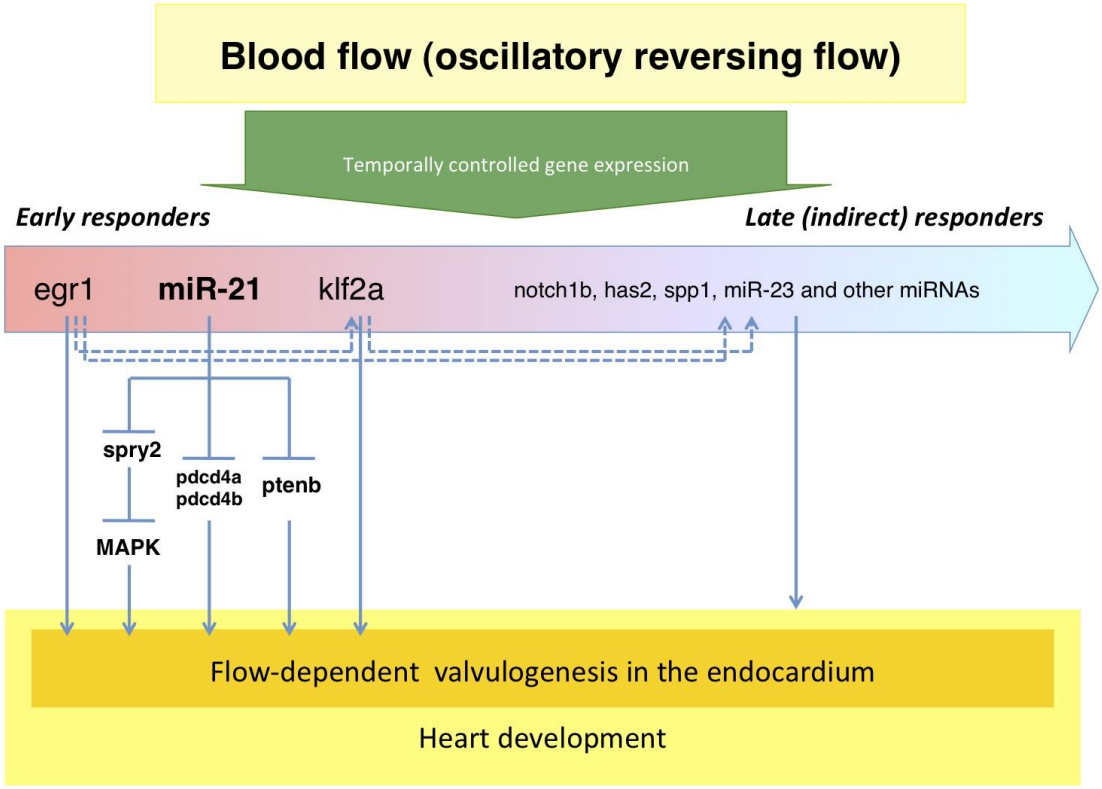

Supplementary Figure S10. A schematic model of the signalling cascade.

A schematic representation of the signalling cascade triggered by the blood flow (especially by the oscillatory reversing flow). The blood flow at the constrictive AV canal applies high mechanical stimuli to the endocardial cells. Such stimuli rapidly induce early responders, such as *miR-21*, *egr1* and *klf2a*. Induced *miR-21* represses its targets (*spry2*, *pdcd4a*, *pdcd4b* and *ptenb*). As a result, MAP kinase signalling is enhanced, and the endocardial cells proliferate to form the valves by combined and simultaneous suppression of the spry2, pdcd4a/b and ptenb functions. Induced egr1 and klf2 regulate their targets that play important roles during valvulogenesis. egr1 might regulate *klf2* and other miRNAs, as reported in mannmals. klf2a also could regulate expression of miRNAs. There might be unknown regulatory cascades that induce other valve-specific genes, such as *notch1b, has2* and *spp1*. Our data highlight the rapid and robust response of *miR-21* triggered by the flow, one of essential steps for the valvulogenesis. Also, we point out that the temporal regulation of hierarchical gene expression contributes to various aspects of the valve formation. In any event, the blood flow is a pivotal trigger for this morphogenetic process**.**